Chemical Geology 267 (2009) 131–138

Contents lists available at ScienceDirect

Chemical Geology

journal homepage: www.elsevier.com/locate/chemgeo

Iron isotope electroplating: Diffusion-limited fractionation

A. Kavner *, A. Shahar, J. Black, E.D. Young

Earth and Space Science Department and Institute for Geophysics and Planetary Physics, UCLA, United States

ARTICLE INFO

Article history:
Accepted 25 April 2009

Editor: ESNL

Keywords:
Electrochemistry
Redox
Diffusion
Stable isotope fractionation
Fe stable isotopes

ABSTRACT

Electron-transfer related isotope fractionation may produce large stable isotope geochemical signatures as a result of a variety of Earth processes, including biology, chemical weathering, fluid–rock interactions, and deep Earth redox reactions. In the laboratory, isotope fractionation at a charged electrode has been observed for electroplating of Fe and Zn; however these can arise from a variety of effects besides the electron transfer process. Here, we examine the effect of mass transport on observed isotope fractionation during potentiostatic electroplating of iron. We examine the observed isotope fractionation as a function of the ratio of the observed plating current to the mass-transport limited current (the Cottrell current). When the electroplating experiments are run at currents greater than the Cottrell current, the observed fractionation is ~−1.15(±0.40) ‰, and the extent of fractionation shows a tendency to decrease with increasing plating rate. When electroplating experiments are run at currents below the Cottrell current, observed fractionations are strongly dependent on the plating rate, with a maximum value of $\delta^{56}Fe = -4.8$. The data set demonstrates that mass transport to the electrode tends to attenuate a large fractionation factor associated with other, non-mass transport, processes at the electrode.

1. Introduction

Redox processes of transition metals often play an active role in many Earth and planetary science processes, such as biological processes, chemical weathering, fluid–rock chemical interactions, and deep Earth chemistry such as reactions during core formation or at the core/mantle boundary. Since the advent of high resolution mass spectrometry techniques to measure ‰ (parts per thousand) variations in stable isotopes abundances, transition metal isotope systems have been used increasingly as geochemical markers for a variety of processes (Albarede and Beard, 2004; Anbar, 2004; Anbar et al., 2005; Anbar and Rouxel, 2007; Beard and Johnson, 2004; Johnson et al., 2004, 2008; Schauble, 2004; Zhu et al., 2002). Specifically, processes that change the valence state of transition metals—redox processes—appear to generate relatively large isotope fractionations, on the order of a few ‰. Redox-related isotope fractionation is predicted in theoretical calculations (Anbar et al., 2005; Jarzecki et al., 2004; Schauble, 2004; Schauble et al., 2001; Polyakov et al., 2007), and observed in laboratory experiments (Anbar et al., 2000; Bullen et al., 2001; Roe et al., 2003), biological systems (Beard et al., 1999; Mandernack et al., 1999; Brantley et al., 2001; Croal et al., 2004; Ohno et al., 2004; Johnson et al., 2005), and ocean (Beard et al., 2003; Rouxel et al., 2005), sedimentary (Johnson et al., 2003; Severmann et al., 2004), and solid Earth (Williams et al., 2004) environments.

Our goal has been to use laboratory electrochemistry techniques to elucidate some of the physical and chemical mechanisms that control redox-related isotope fractionation. In two recent studies, voltage-dependent stable isotope fractionation was observed during potentiostatic electroplating of Fe (Kavner et al., 2005) and Zn (Kavner et al., 2008). During plating of iron, fractionation increased with increasing overpotential (electrochemical driving force). In Zn, the extent of fractionation was larger at lower overpotentials, and decreased with increasing driving force. These results showed large isotope fractionations during the reduction reaction of $M^{2+} + 2e^- = M$ at a negatively charged electrode. The results were interpreted in terms of a modified Marcus equation describing isotopic dependence of electron transfer kinetics (Marcus, 1964, 1965, 1993; Kavner et al., 2005, 2008). This theory, developed for single electron transfer in a homogeneous reaction, assumes that the electron transfer step is the rate-limiting step, and controls the isotope fractionation.

In reality, the behavior at an electrode during electrodeposition is significantly more complicated, with significant variations in solution chemistry adjacent to the double layer and mass transport to the electrode in addition to electron transfer. Each of these steps can generate isotope signatures. For example, Rodushkin et al. (2004) observed iron isotope fractionations on the order of ~−0.3‰ due to diffusion in an aqueous environment. Close to an electrode surface, double-layer models [e.g. Grahame, 1947] predict large local variations in chemistry, such as associated with change in ligands and speciation as the electrode is approached. This can result in isotope signatures associated changes in equilibrium species. This effect can be on the order of a few ~‰ (Hill and Schauble, 2008), and will depend on the

* Corresponding author.
E-mail address: akavner@ucla.edu (A. Kavner).

0009-2541/$ – see front matter © 2009 Elsevier B.V. All rights reserved.
doi:10.1016/j.chemgeo.2009.04.018

solution chemistry and its changes as the electrode surface is approached. Finally, an isotope effect due electron transfer has been hypothesized in two previous papers (Kavner et al., 2005; Kavner et al., 2008).

Our goal in this paper is to examine how isotope fractionation occurs during mass-transport-limited electron transfer processes. We derive an isotope-sensitive version of the Cottrell equation, which describes electrochemical reaction rates in the diffusion-limited regime (Bard and Faulkner, 1980). We use this theory to interpret a series of new experiments showing isotope fractionation during iron electrodeposition under a variety of experimental conditions.

2. Mass transport at an electrode

Mass transfer to a charged electrode is governed by convection, electromigration, and diffusion of the ion species to the surface of the electrode. For simplicity, we only examine the one-dimensional problem. We assume that the electrode is an infinite plane, and all behavior takes place as a function of distance from the electrode. Although these simplifying assumptions may introduce some quantitative errors, they should not change the basic qualitative isotope behavior of these systems. This section follows the development as presented by a standard electrochemistry textbook (Bard and Faulkner, 1980). The steady state, one-dimensional version of the equation governing mass transport to an electrode is known as the Nernst–Planck equation, where total flux is equal to contributions from convection, electromigration, and diffusion, and is given by:

$$J_j(x) = C_j v(x) - \frac{z\mathrm{F}}{\mathrm{RT}} D_j C_j \frac{\partial \varphi}{\partial x} - D_j \frac{\partial C_j(x)}{\partial x} \tag{1}$$

where $J_j(x)$ is the flux of species j to the electrode; C_j is the concentration of species j; $v(x)$ is the viscosity; D_j is the diffusivity of species j; $\partial\varphi/\partial x$ is the electric field, z is the number of electrons transferred in a single reaction (2 for the $Fe^{+2} + 2e^- = Fe$ reaction), T is temperature, R is the ideal gas constant, and F is Faraday's constant, equal to 96,485 Coulombs/mol. This equation can be recast with each flux term written as currents:

$$-zFJ_j(x) = i_{\text{total}} = i_{\text{convection}} + i_{\text{electromigration}} + i_{\text{diffusion}} \tag{2}$$

where $J_i(x)$ is the flux of species j at distance x (units: $s^{-1}\,cm^{-2}$), and the current i is related to the flux via the Faraday equivalent between current and concentration zF; and the terms on the right hand sides of Eqs. (1) and (2) represent currents due to convection, electromigration, and diffusion. Since mass transport by convection cannot generate isotope fractionation by itself, it will not be considered here. In the following two sub-sections, we consider isotope effects of both electromigration and diffusion to a charged electrode.

2.1. Electromigration at an electrode

For simplicity, we assume the electric field varies linearly away from the electrode. The electromigration current is proportional to the electric field, with only concentration and mobility, u_j, as proportionality constants:

$$J_j = u_j c_j \varepsilon \tag{3}$$

The current due to electromigration can then be written as:

$$i_{m,j} = \frac{|z_j| FAu_j C_j \Delta E}{l} \tag{4}$$

where $i_{m,j}$ is the current due to the electromigration of j; $|z_j|$ is the absolute value of the charge on j; F is Faraday's number; A is the area of the electrode; C_j is the concentration of species j; $\Delta\varepsilon$ is the voltage drop across that interface; l is the length scale over which that voltage drop takes place; and u_j is the mobility—which has units of velocity/electric field or cm/s per V/cm or $cm^2\ s^{-1}\ V^{-1}$.

The mobility is derived by considering the force balance between viscous drag and electric field on a charged species in a viscous fluid. At equilibrium, this balance is written as:

$$z_j e\varepsilon = 6\pi\eta r v_j \tag{5}$$

where ε is electric field, η is the viscosity of the fluid, r is the radius of particle, and v is its velocity. The mobility is defined at this equilibrium, as $u_j = v_j/\varepsilon$, where the velocity is the terminal velocity.

$$u_j = \frac{|z_j| e}{6\pi\eta r} \tag{6}$$

Substituting Eq. (6) back into Eq. (4) yields a current due to electromigration equal to:

$$i_{m,j} = \frac{|z_j|^2 FAeC_j \Delta E}{6\pi l \eta r}. \tag{7}$$

The only isotope-dependent term in this equation is related to the concentration of each species C_j. Therefore, although electromigration may change the overall flux to an electrode, it does not cause any additional isotope fractionation that is not already due to other factor affecting relative isotope compositions, such as diffusion, evolution of reservoir, and/or electrochemical processes.

2.2. Diffusion at an electrode

The one-dimensional diffusion equation for a planar electrode is:

$$\frac{\partial C_0(x,t)}{\partial t} = D_0 \frac{\partial^2 C_0(x,t)}{\partial x^2} \tag{8}$$

The initial condition assumes that the concentration near the electrode is identical to the bulk solution; i.e. $C_j(x=0,\ t=0) = C_{j,0}$, where C_0 is the starting concentration in the reservoir. For mass-transport limited processes at an electrode, the concentration at the electrode surface is established by the boundary condition C_j ($x=0$, $t>1$) $=0$ which is equivalent to assuming that at the electrode, the aqueous species is immediately reduced. Finally, we assume that the reservoir is large compared with the amount of plated material, and therefore $C_j(x>>0$, all $t) = C_{j,0}$. As will be seen in the next section, we have designed our experiments to plate out only small amounts of the total ion in solution to satisfy this boundary condition.

The solution to this differential equation with these boundary conditions for mass-transport-limited electrochemical reactions provides the current-time response at an electrode, and is known as the Cottrell equation (Bard and Faulkner, Section 5.2.1).

$$i(t) = i_{\mathrm{d}}(t) = \frac{nFA\sqrt{D_0}}{\sqrt{\pi t}} \tag{9}$$

where $i_{\mathrm{d}}(t)$ is the rate-limiting current, also known as the "Cottrell current"; and A is the electrode area. When reaction rates are significantly larger than the Cottrell current, then mass transport to the electrode is the rate-limiting step. If experimental electrochemical reaction rates are much lower than the Cottrell current, then material can be supplied to the electrode fast enough so that another electrode processes is rate-limiting. Typical values of time-dependent Cottrell currents for 2 M and 0.25 M $FeCl_2$ solutions—such as the one we use in our experiments—are plotted in Fig. 1, along with our estimated experimental plating currents (cf. Section 3).

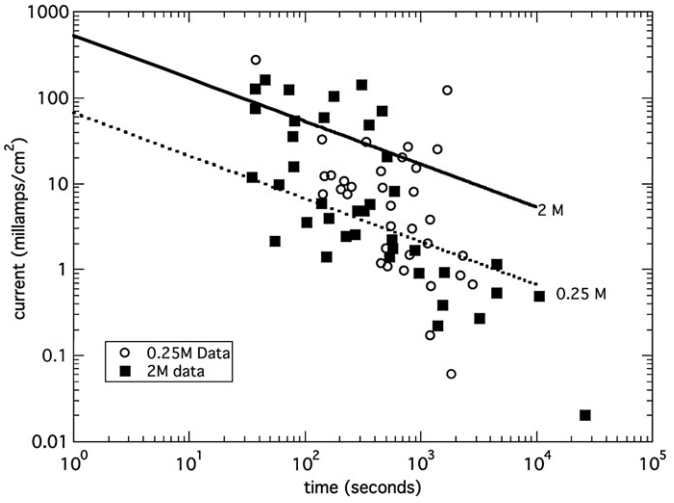

Fig. 1. Electrodeposition rate (current) as a function of total plating time for each experiment for 2 M (solid squares) and 0.25 M (open circles) $FeCl_2$ solutions. Straight lines show the calculated Cottrell (mass-transport limiting) current calculated for 2 M (solid) and 0.25 M (dashed) $FeCl_2$ solutions, using $i(t) = i_d(t) = \frac{nFA\sqrt{D_0}}{\sqrt{\pi t}}$ with $D_0 = 6\times10^{-6}$ cm^2/s and $A = 1$ cm^2.

The isotope-dependent Cottrell equation reduces to:

$$\delta^2 M = 1000\left(\sqrt{\frac{D_{0,2}}{D_{0,2}}} - 1\right) \tag{10}$$

where ^2M is the isotope fractionation of the metal's heavy isotope (M,2) with respect to its light isotope. The diffusivities of the two isotopologues are $D_{0,2}$ for the heavy isotope and $D_{0,1}$ for the light. Eq. (10) predicts a time-independent fractionation factor during mass-transport limited electroplating.

These equations for mass transport at an electrode suggest that isotope fractionation will be a constant related only to the diffusivity of the species in solution at the electrode. Although the concentrations of the species adjacent to the electrode varies as a function of time according to these solutions to the diffusion equation, the ratio of the concentrations of the two isotopes themselves do not vary as a function of time. Therefore, fractionation by diffusive transport is predicted to be a constant, even if the kinetics of the reaction changes due to application of overpotential. Rodushkin et al. (2004) measured a fractionation factor (α) due to diffusion of iron isotopes in aqueous systems equal to $D^{56}Fe/D^{54}Fe - 1 = -9\times10^{-5}$, and observed isotope fractionations in their experimental system up to −0.3‰.

3. Experimental procedure

3.1. Electroplating experiments

The goal of the experiments is to perform a series of Fe electrodeposition experiments under a variety of controlled potential conditions, and to examine how the isotope composition of the electroplated iron metal varies as a function of the ratio of the electrodeposition rate to the calculated mass-transport limited current. Eight sets of electrodeposition experiments were performed, as outlined in Table 1. In all cases, Fe metal was electroplated from $FeCl_2$ starting solutions, with concentrations varying from 2 M down to 0.125 M. In all cases, plating solutions were acidified with 1 M HCl.

The experimental procedure follows a similar approach to what was reported in Kavner et al. (2005). Iron electroplating experiments were performed under potentiostatic (constant voltage) conditions with an Autolab Potentiostat using a three-electrode electrochemical cell, equipped with a silver/silver chloride reference electrode. All data are tabled in Table 1. For each plating experiment, a 50 mL aliquot was poured from initial 1 L stock solutions. Prior to each experiment, the solution was de-oxygenated by bubbling Ar for 20 min. Both the working electrode (where electrodeposition occurs), and the counter electrode consisted of ~1 cm^2 plates of amorphous carbon (Alfa Aesar). Cell potentials are reported with respect to the calculated equilibrium reduction potential of the Fe^{+2}/Fe_M reaction using the Nernst equation. Following convention, we define our electrodeposition potentials as negative values. Values ranged from −0.25 V to −1.53 V. The total charge (Q) passed during each deposition experiment was also controlled, with values from $Q = 1$ to 99 C. In all experiments, iron deposition was accompanied by a significant hydrogen evolution at the working electrode. Therefore, not all of the Coulombs passed resulted in deposition of iron. As described in the next section, dilutions of collected material provided an estimate of the reaction efficiency, which varied throughout the experiments, from less than 1% to almost 100%. Aside from mixing at the electrode due to hydrogen evolution, the solution was not mixed during deposition experiments, and temperature was not controlled during these experiments. For experiment series A–G, less than 0.1% of the total iron in the solution was electroplated during each experiment in order to avoid evolution of the isotopic composition of the plating solution reservoir.

3.2. Mass spectrometry

Isotopic analysis of the plated material and remaining solution was performed following the procedures reported in Kavner et al. (2005). An effort was made to collect all of the deposited material from each electrode. Each electrode was collected and gently washed with distilled water to remove the excess plating bath solution. The electrodes were then placed in clean Teflon beakers. Electroplated iron was removed from the electrodes with hot concentrated HNO_3 acid for about 6 h followed by hot concentrated HCl acid for about 10 h. Subsequent scanning electron microscopy examination of cleaned electrodes showed no remaining iron and a small amount of increase in the roughness of the electrode surface. All solutions were dried down after acid baths, and were finally re-dissolved in 0.3 N nitric acid for analysis. In addition, for each set of experiments, a small amount of the starting solution was dissolved in hot concentrated HNO_3 acid and then diluted to 0.3 N for analysis. The samples were diluted to Fe concentrations ranging from 3 to 5 ppm. Dilutions were recorded to provide an estimate of the amount of material collected from the electrode, in milligrams (Table 1). This is likely a lower bound to the actual amount plated, and we estimate a factor of ~2 uncertainty in the estimate. This value was used to estimate the electroplating current, via the formula i_{deop} (milliamps) $= 1000\times zFg_{plated}/(W\,t)$ where $z = 2$ electrons transferred, F is Faraday's constant = 96,485 C/mol, g_{plated} is the amount of material plated, W is the atomic mass of Fe, equal to 55.56 g/mol, and t is the total amount of time for the electrodeposition experiment. These values, which vary from 10 s of μA to 10 s of mA, are shown in Table 1. The ratio of this value to the total amount of current passed in the experiment ($= Q/t$, where Q is the total amount of Coulombs passed in each experiment, and is shown in Table 1) provides a lower-bound estimate to the efficiency of the iron electroplating reaction with respect to hydrogen evolution at the electrode. Estimated efficiencies were highly variable among individual experiments, and between sets of experiments, with many values in the 0.1% and 10% ranges. For each experiment, an estimated plating rate in mol/m^2/s is calculated using the relation rate $= (i/AzF)$ where i is the estimated plating current in amps and A is the electrode area in m^2. We consider these values in plating rate to be order-of-magnitude estimates, given sources of uncertainty in the estimate of plating current and uncertainty in electrode area, which was not monitored directly for these experiments, but in all cases was approximately ~1 cm^2.

Table 1
Data summary from all plating experiments.

Experiment set	[$FeCl_2$]	Plating overpotential (V)	Charge passed (C)	Time (s)	δ^{56}Fe (‰ wrt starting solution)[b]	δ^{67}Fe (‰ wrt starting solution)[b]	Fe deposition reaction efficiency (%)[c]	Calculated plating current (mA)	Calculated Cottrell limit (mA)	Plating current/ Cottrell current
From Kavner et al. 2005	2	-0.62	95	4508	-1.36(5)	-2.06(5)	5.46	1.15	7.95	0.15
	2	-0.27	82	10,600	-0.07(4)	-0.10(10)	6.32	0.49	5.18	0.09
	2	-1.37	80	540	-2.12(1)	-3.11(4)	0.94	1.39	22.96	0.06
	2	-0.87	99	970	-1.58(1)	-2.34(5)	0.88	0.90	17.13	0.05
	2	-0.27	50	26,330	0.06(2)	0.10(2)	0.94	0.02	3.29	0.01
	2	-0.62	80	1550	-1.51(2)	-2.25(5)	0.74	0.38	13.55	0.03
	2	-0.47	95	3210	-0.48(2)	-0.70(5)	0.92	0.27	9.42	0.03
	2	-0.62	77	1400	-0.37(3)	-0.54(6)	0.40	0.22	14.26	0.02
A	2	-0.62	80	473	-3.29(13)	-4.86(22)	n/a	n/a	24.52	n/a
	2	-0.27	10	2400	-2.15(11)	-3.15(16)	n/a	n/a	10.89	n/a
	2	-1.37	80	160	-3.39(4)	-5.02(6)	n/a	n/a	42.15	n/a
	0.5	-1.35	80	402	-1.99(2)	-2.91(7)	n/a	n/a	6.64	n/a
	0.5	-0.6	80	933	-1.40(2)	-2.07(6)	n/a	n/a	4.37	n/a
	0.5	-0.25	1	12,000	-0.47(4)	-0.44(9)	n/a	n/a	1.22	n/a
B	0.125	-1.53	80	n/a	-0.19(7)	-0.36(10)	n/a	n/a	n/a	n/a
	0.125	-1.03	10	445	-0.18(3)	-0.28(33)	40.65	9.18	1.58	5.78
	0.125	-0.83	10	n/a	-0.21(9)	-0.28(16)	34.55	n/a	n/a	n/a
	0.125	-0.63	10	n/a	-0.24(10)	-0.29(9)	19.74	n/a	n/a	n/a
	0.125	-0.43	10	n/a	-0.57(5)	-0.88(8)	17.28	n/a	n/a	n/a
	0.5	-1.25	10	114	-0.66(6)	-1.00(13)	46.07	40.59	12.49	3.24
	0.5	-0.85	10	263	-0.79(5)	-1.16(8)	27.64	10.56	8.22	1.28
	0.5	-1.05	10	147	-0.66(10)	-1.00(20)	36.85	25.18	11.00	2.28
	0.5	-0.65	10	367	-1.11(8)	-1.67(4)	27.64	7.57	6.96	1.08
	0.5	-0.45	10	634	-1.36(3)	-2.06(5)	22.11	3.50	5.30	0.66
	0.5	-1.05	80	738	-0.87(1)	-1.28(14)	33.17	36.12	4.91	7.32
	2	-1.27	10	37	-1.54(8)	-2.21(21)	27.64	75.04	87.71	0.85
	2	-0.87	10	79	-1.66(3)	-2.39(43)	27.64	35.15	60.02	0.58
	2	-0.47	10	228	-1.88(4)	-2.76(12)	5.53	2.44	35.33	0.07
	2	-1.07	10	45	-0.79(10)	-1.20(20)	71.87	160.42	79.53	2.01
C	2	-1.37	80	307	-1.33(4)	-1.97(2)	54.23	141.31	30.45	4.64
	2	-1.37	40	177	-1.62(11)	-2.40(6)	46.01	103.98	40.10	2.59
	2	-1.37	20	72	-1.55(6)	-2.28(3)	44.88	124.67	62.87	1.98
	2	-1.37	10	37	-1.47(3)	-2.21(8)	47.33	127.91	87.71	1.46
	2	-0.77	80	463	-1.92(2)	-2.83(8)	40.67	70.28	24.79	2.83
	2	-0.77	40	357	-1.75(9)	-2.62(13)	43.38	48.61	28.24	1.72
	2	-0.77	20	147	-1.57(5)	-2.34(11)	43.38	59.03	44.00	1.34
	2	-0.77	10	81	-1.57(2)	-2.36(1)	43.38	53.56	59.28	0.90
D	0.25	-0.59	80	2314	-1.67(4)	-2.49(7)	4.13	1.43	1.39	1.03
	0.25	-0.59	40	1160	-1.69(3)	-2.52(3)	5.78	1.99	1.96	1.02
	0.25	-0.59	20	552	-1.27(2)	-1.88(7)	8.67	3.14	2.84	1.11
	0.25	-0.59	10	455	-1.70(3)	-2.53(4)	5.33	1.17	3.13	0.38
	0.25	-0.84	80	1220	-1.53(3)	-2.27(2)	5.78	3.79	1.91	1.99
	0.25	-0.84	40	472	-1.06(1)	-1.59(4)	10.40	8.82	3.07	2.87
	0.25	-0.84	20	255	-0.99(2)	-1.48(3)	11.55	9.06	4.17	2.17
	0.25	-0.84	10	149	-0.95(8)	-1.38(7)	17.75	11.99	5.47	2.19
	0.25	-1.09	80	877	-1.21(2)	-1.77(4)	8.67	7.91	2.25	3.51
	0.25	-1.09	40	553	-1.17(2)	-1.78(4)	7.54	5.46	2.84	1.92
	0.25	-1.09	20	220	-1.03(4)	-1.54(2)	11.55	10.54	4.50	2.34
	0.25	-1.09	10	144	-0.98(4)	-1.45(2)	10.65	7.44	5.56	1.34
E	2	-0.62	80	566	-3.90(4)	-5.77(4)	1.58	2.23	22.42	0.10
	2	-0.62	80	570	-3.18(6)	-4.73(8)	1.24	1.74	22.34	0.08
	2	-0.62	40	272	-3.28(3)	-4.89(9)	1.74	2.55	32.35	0.08
	2	-0.62	20	154	-2.51(5)	-3.74(6)	1.08	1.41	42.99	0.03
	2	-0.62	10	80	-2.90(3)	-4.31(4)	12.62	15.70	59.50	0.26
	2	-0.87	80	322	-3.56(4)	-5.27(9)	1.93	4.79	29.74	0.16
	2	-0.87	40	162	-3.54(1)	-5.27(4)	1.60	3.96	41.90	0.09
	2	-0.87	20	104	-3.60(2)	-5.37(4)	1.82	3.53	52.44	0.07
	2	-0.87	10	55	-3.67(2)	-5.48(8)	1.15	2.11	72.00	0.03
	2	-1.12	80	286	-3.65(5)	-5.43(6)	1.73	4.85	31.54	0.15
	2	-1.12	40	140	-3.68(5)	-5.51(14)	2.04	5.84	45.12	0.13
	2	-1.12	20	60	-2.76(6)	-4.12(3)	2.88	9.61	68.76	0.14
	2	-1.12	10	35	-1.70(2)	-2.54(2)	4.08	11.70	89.79	0.13

Table 1 (*continued*)

Experiment set	[$FeCl_2$]	Plating overpotential (V)	Charge passed (C)	Time (s)	δ^{56}Fe (‰ wrt starting solution)[b]	δ^{67}Fe (‰ wrt starting solution)[b]	Fe deposition reaction efficiency (%)[c]	Calculated plating current (mA)	Calculated Cottrell limit (mA)	Plating current/ Cottrell current
	0.25	-0.54	80	2216	-2.97(9)	-4.38(9)	2.37	0.85	1.42	0.60
	0.25	-0.59	80	2820	-3.19(4)	-4.73(19)	2.37	0.67	1.26	0.53
	0.25	-1.24	80	914	-1.51(12)	-2.26(16)	17.35	15.19	2.21	6.89
	0.25	-0.94	80	811	-1.50(6)	-2.24(5)	1.48	1.46	2.34	0.62
	0.25	-1.09	80	694	-1.50(5)	-2.22(7)	17.35	20.00	2.53	7.90
	0.25	-0.74	80	1230	-2.65(8)	-3.85(12)	0.98	0.63	1.90	0.33
F	2	-0.47	80	884	-4.65(3)	-6.92(14)	1.86	1.68	17.94	0.09
	2	-0.37	80	1596	-4.81(7)	-7.19(10)	1.86	0.93	13.35	0.07
	2	-0.27	80	4504	-4.63(12)	-6.89(26)	2.98	0.53	7.95	0.07
	2	-0.57	80	593	-4.55(4)	-6.74(17)	5.97	8.05	21.91	0.37
	2	-0.67	80	512	-4.30(5)	-6.27(19)	13.02	20.34	23.58	0.86
	2	-0.77	80	363	-2.41(6)	-3.61(9)	2.60	5.74	28.00	0.20
	0.25	-1.44	20	169	-1.11(7)	-1.71(9)	10.41	12.32	5.13	2.40
	0.25	-0.74	20	501	-1.94(12)	-2.86(20)	4.34	1.73	2.98	0.58
	0.25	-1.24	20	235	-1.63(12)	-2.44(8)	8.68	7.38	4.35	1.70
	0.25	-1.34	20	206	-1.36(8)	-2.04(20)	8.68	8.44	4.65	1.81
G	0.25	-0.64	20	721	-1.90(6)	-2.81(14)	3.47	0.96	2.48	0.39
	0.25	-0.59	20	516	-2.33(10)	-3.35(20)	2.78	1.08	2.94	0.37
	0.25	-0.44	20	1208	-1.51(13)	-2.20(11)	1.04	0.17	1.92	0.09
	0.25	-0.34	20	1843	-2.79(6)	-4.17(21)	0.58	0.06	1.55	0.04
	0.25	-1.09	20	142	-0.64(5)	-1.10(10)	23.14	32.59	5.60	5.82
	0.25	-1.09	44	340	-0.78(5)	-1.30(6)	23.66	30.62	3.62	8.47
	0.25	-1.09	92	782	-0.91(7)	-1.46(36)	22.63	26.63	2.38	11.17
	0.25	-1.09	131	1400	-1.03(11)	-1.75(10)	26.49	24.79	1.78	13.91
H	0.25	-1.09	44	455	-0.99(5)	-1.41(48)	14.20	13.73	3.13	4.39
	0.25	-1.09	n/a	1700	-0.98(16)	-1.61(16)	n/a	122.49	1.62	n/a
	0.25	-1.09	44	38	-0.78(48)	-1.18(10)	23.66	274.00	10.82	25.33
	0.25	-1.09	44	841	-0.66(12)	-1.10(28)	5.63	2.95	2.30	1.28

[a]calculated with respect to starting solution, referenced to standard reduction potential adjusted to Fe concentration using Nernst's law.
[b]two-sigma errors are reported.
[c]efficiency calculated by…
[d]Ratio of the observed average current/Cottrell average current.

The Fe isotopic compositions of plating experiments were determined by sample-standard comparisons using a multi-collector inductively–coupled plasma source mass spectrometer (MC–ICPMS) (ThermoFinnigan Neptune) at UCLA. Solutions were found to be effectively pure; trace amounts of ^{52}Cr, the most abundant Cr isotope (>83%), were negligible; there was no measurable mass interference at mass 54 (e.g., background ^{52}Cr signals of 5 mV corresponding to a 0.1 mV ^{54}Cr background signal compared with sample ^{54}Fe signals of several volts). Peak heights for sample and standard were matched to minimize background effects. The required dilutions for each Fe sample were recorded to provide estimates of the amount of Fe electroplated in each experiment. Mass interferences from ArO^+, $ArOH^+$ and ArN^+ were resolved from the ^{56}Fe, ^{57}Fe and ^{54}Fe peaks by operating at a mass resolving power of ~12,000 (corresponding to a flat-top peak mass resolution of 4000). Each solution was analyzed 5 to 6 times. All isotope measurements and their two-sigma error bars are reported in reference to the isotopic composition of the stock solutions. We report ^{56}Fe/^{54}Fe and ^{57}Fe/^{54}Fe of reactant and product Fe as the per mil deviations from isotope ratio of the starting material using the δ notation where:

$$\delta^{56}\mathrm{Fe} = (((^{56}\mathrm{Fe}/^{54}\mathrm{Fe})\mathrm{sample}/(^{56}\mathrm{Fe}/^{54}\mathrm{Fe})_{\mathrm{Starting\ solution}}) - 1) * 1000$$

and

$$\delta^{57}\mathrm{Fe} = (((^{57}\mathrm{Fe}/^{54}\mathrm{Fe})\mathrm{sample}/(^{57}\mathrm{Fe}/^{54}\mathrm{Fe})_{\mathrm{Starting\ solution}}) - 1) * 1000.$$

Mean values for δ^{56}Fe and their corresponding two-sigma error bars are reported in Table 1.

4. Results and discussion

In all cases, the light isotopes of iron are preferentially electroplated, with observed fractionations varying up to $\delta^{56}\mathrm{Fe} = -4.8$ (± 0.02) ‰. A three-isotope plot (Fig. 2) shows that the data fall on a mass-dependent fractionation line. A weighted linear fit to the data provides a β slope of 0.671($\pm$0.004) (For fitting procedures see Young et al. (2002)). This value is in excellent agreement with an earlier β measurement of 0.672 (0.003) (Kavner et al., 2005), and is consistent with a kinetic fractionation process involving unsolvated or singly-solvated Fe^{+2} (inset, Fig. 2).

Fig. 1 shows that the experimental currents cluster around the calculated Cottrell currents for mass-transport limited electroplating, with some falling above the Cottrell threshold, and some falling below. Since the Cottrell current is dependent on solution concentration, data for the concentrated (2 M) starting solutions and dilute (0.25 M) starting solutions are labeled separately. We observe that in the experiments with the more concentrated solutions, more of the results are below the mass-transport limiting current. Fig. 1 also shows that estimated electroplating currents for the experiments were highly variable over several orders of magnitude. This variability was mostly by design—the electrodeposition rate is an activated process exponentially dependent on the applied voltage, which was varied in these experiments, as shown in Fig. 3. Fig. 3 also shows that even at a single overpotential, the estimated deposition rates vary over several orders of magnitude. This is likely due to a combination of factors, especially the large degree of uncertainty in estimating the iron deposition rate, variations in electrodeposition efficiency (with respect to hydrogen evolution) from experiment to experiment, and variability in starting solution concentrations.

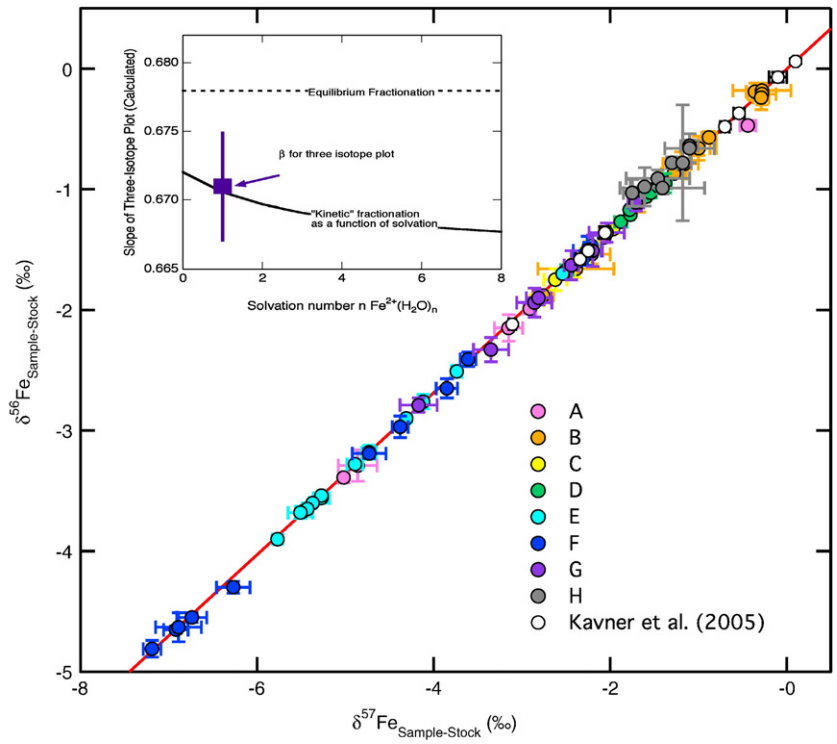

Fig. 2. All iron electrodeposition data on a three-isotope plot, with two-sigma error bars. Our best fit β value (See Young et al. (2002)) is equal to 0.671 ($\pm$0.004), shown in red. The inset shows the measured β value (purple square) in comparison with calculated β values for equilibrium fractionation (dotted line) and for kinetic processes involving hydrated Fe^{+2} species as a function of solvation number (solid black line). (For interpretation of the references to colour in this figure legend, the reader is referred to the web version of this article.)

The relationship between the experimental current and the calculated Cottrell current enables the data to be sorted into two regimes. Fig. 4 shows the measured isotope fractionation as a function of the ratio of the estimated electroplating current to the calculated Cottrell current for each plating experiment. When this ratio is much greater than 1, the plating kinetics are likely to be limited by mass transport to the electrode. When the ratio is much less than 1, the overall plating kinetics are governed by electrode processes. Close to 1, mass transport and electrode processes likely compete to govern the overall kinetics. Fig. 4 shows that the fractionation—although scattered—shows different trends within each regime. In the next paragraphs, we consider each regime separately.

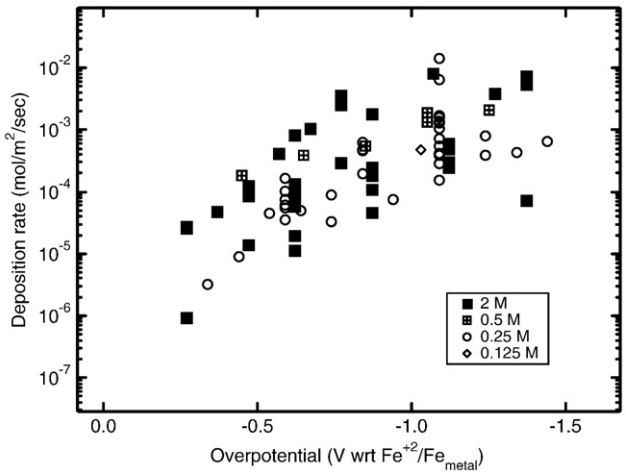

Fig. 3. Estimated deposition rate as a function of applied overpotential in the electroplating experiments.

When the estimated experimental current is above the Cottrell current, the resultant observed isotope fractionation decreases weakly with increasing rate (current), with measured δ^{56}Fe clustered about values varying from -1.5‰ to -1‰. As shown in Fig. 4, fractionation factor measured for diffusion processes by Rodushkin et al. (2004) is much lower than our observations in the mass-transport limited regime, though diffusion processes may be helping to place a lower bound on our observed fractionations.

To examine trends of fractionation in the non mass-transport-limited regime, we plot isotope fractionation as a function of plating rate only for the data where the plating current is less than 50% of the Cottrell limiting current (Fig. 5). Given the order-of-magnitude level of uncertainty in our estimated plating rate, with this data set we cannot deconvolve possible effects of fractionation as a function of time, voltage, current, or charge passed. However, the data suggest that for the dilute starting solutions, fractionation is approximately constant with plating rate, with values from -1.5‰ to -2.75‰. Isotope fractionations from the more concentrated solutions are significantly more varied, with the trend showing that the extent of fractionation general increases as a function of plating rate. This result is in agreement with the original study of Kavner et al. (2005). Indeed, all of the data in that study were performed under conditions of low current with respect to the Cottrell current (Table 1). The results in Figs. 4 and 5 suggest that mass-transport limited kinetics is damping down an isotope signature that would be much larger, in the extreme of fast diffusion to an electrode. Although the data are consistent with the hypothesis proposed in Kavner et al. (2005) and Kavner et al. (2008) that rate-dependent isotope fractionation is expected in electron transfer conditions, this current data set is not able to explicitly test this hypothesis.

Also plotted in Fig. 5 are the predicted equilibrium isotope exchanges between different species in solution (e.g. Schauble et al., 2001), which range from $+0.9$ for equilibrium partitioning between $Fe^{+2}[H_2O]_6$ and Fe_{metal}, to -1.3 for $Fe^{+2}[Cl^{-1}]_4$–Fe_{metal} to -2.2 for

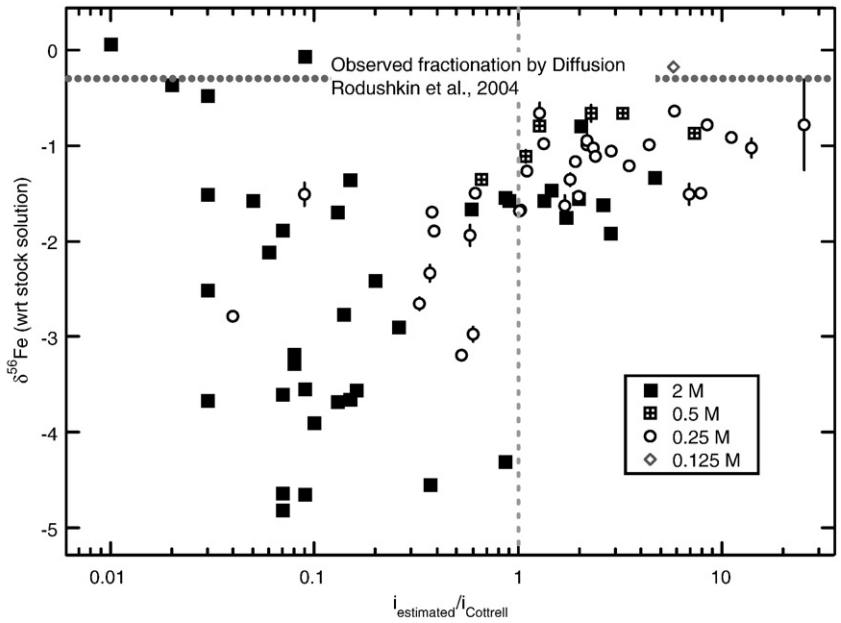

Fig. 4. Plot of fractionation as a function of the ratio of the estimated iron electroplating current to the average diffusion-limiting current. The vertical dashed line separates mass-transport limited regime (to the right of the plot) and the electron transfer limited regime (to the left). Thin horizontal dashed gray line shows the measured isotope fractionation factor due to diffusion measured by Rodushkin et al. (2004).

$Fe[Cl^{-1}]_4$–$Fe^{+2}[H_2O]_6$ equilibrium. An analysis of the starting solutions using PHREEQ predicts that $Fe^{+2}[Cl^-]_4$ compounds predominate in the concentrated 2 M solutions; while $Fe^{+2}[H_2O]_6$ dominates in the 0.5, 0.25, and 0.125 solutions. Isotope fractionations due to changes in speciation may occur as the electrode double layer is approached. However, the data shown in Fig. 5 suggest that there is no single equilibrium speciation isotope effect dominating the observations. To fully test whether speciation changes are responsible for the observed isotope signature, the data need to be tested against a reservoir box-model that elucidates changes in chemical speciation adjacent to an electrified interface, and calculates the associated isotope effect.

5. Conclusions

Several conclusions are apparent from the data and analysis in terms of mass-transport limited kinetics. First, diffusion-limited mass transport is definitely playing a role at an electrode. Second, for the experiments where we are confident that the currents are above the limiting current, the isotope effects are smaller than when the currents are low enough to be below the diffusion-limited regime. Our observed fractionations in the diffusion-limited regime are consistent with Rodushkin et al.'s measurements of Fe^{2+} ion isotope separation during diffusion. We also note that the fractionations observed during experiments not limited by diffusion are highly

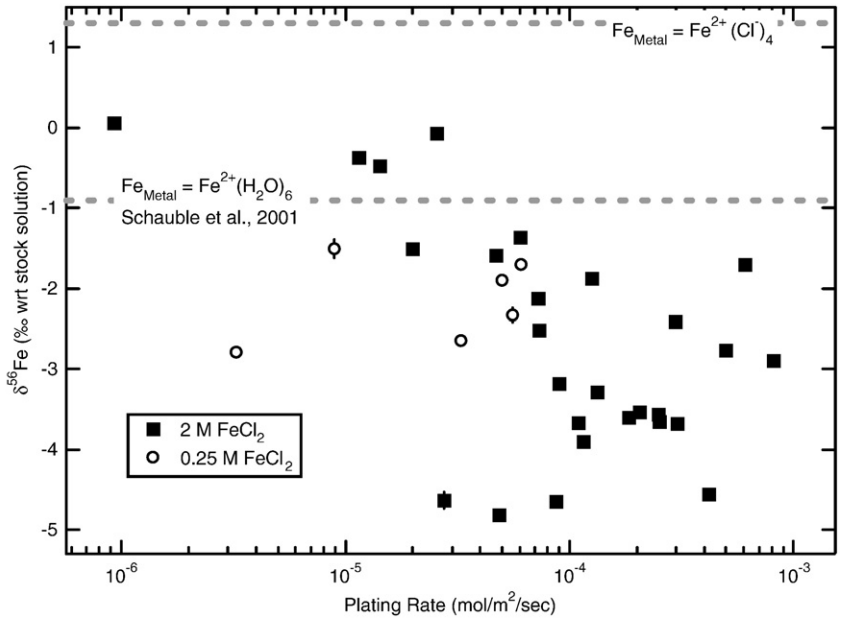

Fig. 5. Plot of iron isotope fractionation with respect to plating solution versus the plating rate in $mol/m^2/s$ for data where the plating current was less than half of the Cottrell current. Black squares are from the 2 M stock solution and open circles are from the 0.25 M stock solution. 2σ error bars often fall within marker size. Thick horizontal dashed lines show calculated equilibrium fractionation factors between iron species in solution and the metal phase [Schauble et al., 2001].

varied, and often significantly larger. These observations strongly suggest that the electron transfer process itself is responsible for large isotope separations, unrelated to the effects of diffusion. Finally, since the data are quite scattered, the data show us that experiments under well-controlled conditions—including temperature and mass transport–are required in order to test the hypothesis of a voltage-dependent fractionation effect due solely to processes at the electrode.

Acknowledgements

We acknowledge illuminating conversations with Edwin Schauble and Pam Hill. AK and AS acknowledge support from the NASA Exobiology under grant number NNG05GQ92G.

References

Albarede, F., Beard, B., 2004. Analytical methods for non-traditional isotopes, geochemistry of non-traditional stable isotopes. Reviews in Mineralogy & Geochemistry 113–152.
Anbar, A.D., 2004. Iron stable isotopes: beyond biosignatures. Earth and Planetary Science Letters 217 (3–4), 223–236.
Anbar, A.D., Rouxel, O., 2007. Metal stable isotopes in paleoceanography. Annual Review of Earth and Planetary Sciences 35, 717–746.
Anbar, A.D., Roe, J.E., Barling, J., Nealson, K.H., 2000. Nonbiological fractionation of iron isotopes. Science 288 (5463), 126–128.
Anbar, A.D., Jarzecki, A.A., Spiro, T.G., 2005. Theoretical investigation of iron isotope fractionation between Fe(H2O)(3+)(6) and Fe(H2O)(2+)(6): Implications for iron stable isotope geochemistry. Geochimica Et Cosmochimica Acta 69 (4), 825–837.
Bard, A.J., Faulkner, L.R., 1980. Electrochemical Methods, Fundamentals and Applications. Wiley, New York. 718 pp.
Beard, B.L., Johnson, C.M., 2004. Fe isotope variations in the modern and ancient earth and other planetary bodies, geochemistry of non-traditional stable isotopes. Reviews in Mineralogy & Geochemistry 319–357.
Beard, B.L., et al., 1999. Iron isotope biosignatures. Science 285 (5435), 1889–1892.
Beard, B.L., Johnson, C.M., Von Damm, K.L., Poulson, R.L., 2003. Iron isotope constraints on Fe cycling and mass balance in oxygenated Earth oceans. Geology 31 (7), 629–632.
Brantley, S.L., Liermann, L., Bullen, T.D., 2001. Fractionation of Fe isotopes by soil microbes and organic acids. Geology 29 (6), 535–538.
Bullen, T.D., White, A.F., Childs, C.W., Vivit, D.V., Schulz, M.S., 2001. Demonstration of significant abiotic iron isotope fractionation in nature. Geology 29 (8), 699–702.
Croal, L.R., Johnson, C.M., Beard, B.L., Newman, D.K., 2004. Iron isotope fractionation by Fe(II)-oxidizing photoautotrophic bacteria. Geochimica Et Cosmochimica Acta 68 (6), 1227–1242.
Grahame, D.C., 1947. The electrical double layer and the theory of electrocapillarity. Chemical Reviews 41, 441–501.
Hill, P.S., Schauble, E.A., 2008. Modeling the effects of bond environment on equilibrium iron isotope fractionation in ferric aquo-chloro complexes. Geochimica Et Cosmochimica Acta 72 (8), 1939–1958.
Jarzecki, A.A., Anbar, A.D., Spiro, T.G., 2004. DFT analysis of Fe(H2O)(6)(3+) and Fe (H2O)(6)(2+) structure and vibrations; implications for isotope fractionation. Journal of Physical Chemistry A 108 (14), 2726–2732.
Johnson, C.M., Beard, B.L., Beukes, N.J., Klein, C., O'Leary, J.M., 2003. Ancient geochemical cycling in the Earth as inferred from Fe isotope studies of banded iron formations from the Transvaal Craton. Contributions to Mineralogy and Petrology 144 (5), 523–547.
Johnson, C.M., Beard, B.L., Albarede, F., 2004. Overview and general concepts, geochemistry of non-traditional stable isotopes. Reviews in Mineralogy & Geochemistry 1–24.
Johnson, C.M., Roden, E.E., Welch, S.A., Beard, B.L., 2005. Experimental constraints on Fe isotope fractionation during magnetite and Fe carbonate formation coupled to dissimilatory hydrous ferric oxide reduction. Geochimica Et Cosmochimica Acta 69 (4), 963–993.
Johnson, C.M., Beard, B.L., Roden, E.E., 2008. The iron isotope fingerprints of redox and biogeochemical cycling in the modern and ancient Earth. Annual Review of Earth and Planetary Sciences 36, 457–493.
Kavner, A., Bonet, F., Shahar, A., Simon, J., Young, E., 2005. The isotopic effects of electron transfer: an explanation for Fe isotope fractionation in nature. Geochimica Et Cosmochimica Acta 69 (12), 2971–2979.
Kavner, A., John, S.G., Sass, S., Boyle, E.A., 2008. Redox-driven stable isotope fractionation in transition metals: application to Zn electroplating. Geochimica Et Cosmochimica Acta 72 (7), 1731–1741.
Mandernack, K.W., Bazylinski, D.A., Shanks, W.C., Bullen, T.D., 1999. Oxygen and iron isotope studies of magnetite produced by magnetotactic bacteria. Science 285 (5435), 1892–1896.
Marcus, R., 1964. Chemical and electrochemical electron-transfer theory. Annual Review of Physical Chemistry 15, 155–196.
Marcus, R.A., 1965. On the theory of electron-transfer reactions. VI. Unified treatment for homogeneous and electrode reactions. Journal of Chemical Physics 43 (2), 679–701.
Marcus, R.A., 1993. Electron-transfer reactions in chemistry – theory and experiment. Reviews of Modern Physics 65 (3), 599–610.
Ohno, T., Shinohara, A., Kohge, I., Chiba, M., Hirata, T., 2004. Isotopic analysis of Fe in human red blood cells by multiple collector–ICP-mass spectrometry. Analytical Sciences 20 (4), 617–621.
Polyakov, V.B., Clayton, R.N., Horita, J., Mineev, S.D., 2007. Equilibrium iron isotope fractionation factors of minerals: reevaluation from the data of nuclear inelastic X-ray scattering and Mossbauer spectroscopy. Geochim. Cosmochim. Acta 71, 3833–3846.
Rodushkin, I., Stenberg, A., Andren, H., Malinovsky, D., Baxter, D.C., 2004. Isotopic fractionation during diffusion of transition metal ions in solution. Analytical Chemistry 76 (7), 2148–2151.
Roe, J.E., Anbar, A.D., Barling, J., 2003. Nonbiological fractionation of Fe isotopes: evidence of an equilibrium isotope effect. Chemical Geology 195 (1–4), 69–85.
Rouxel, O.J., Bekker, A., Edwards, K.J., 2005. Iron isotope constraints on the Archean and Paleoproterozoic ocean redox state. Science 307 (5712), 1088–1091.
Schauble, E.A., 2004. Applying stable isotope fractionation theory to new systems, geochemistry of non-traditional stable isotopes. Reviews in Mineralogy & Geochemistry 65–111.
Schauble, E.A., Rossman, G.R., Taylor, H.P., 2001. Theoretical estimates of equilibrium Fe-isotope fractionations from vibrational spectroscopy. Geochimica Et Cosmochimica Acta 65 (15), 2487–2497.
Severmann, S., et al., 2004. The effect of plume processes on the Fe isotope composition of hydrothermally derived Fe in the deep ocean as inferred from the Rainbow vent site, Mid-Atlantic Ridge, 36 degrees 14′ N. Earth and Planetary Science Letters 225 (1–2), 63–76.
Williams, H.M., et al., 2004. Iron isotope fractionation and the oxygen fugacity of the mantle. Science 304 (5677), 1656–1659.
Young, E.D., Galy, A., Nagahara, H., 2002. Kinetic and equilibrium mass-dependent isotope fractionation laws in nature and their geochemical and cosmochemical significance. Geochimica Et Cosmochimica Acta 66 (6), 1095–1104.
Zhu, X.K., et al., 2002. Mass fractionation processes of transition metal isotopes. Earth and Planetary Science Letters 200 (1–2), 47–62.